The carbon economics of vegetative phase change: why plants make juvenile and adult leaves

Erica Lawrence (lawrence.erica.h@gmail.com)
University of Pennsylvania https://orcid.org/0000-0002-0220-3210
Clint Springer
Saint Joseph's University
Brent Helliker
University of Pennsylvania
Scott Poethig
University of Pennsylvania

Article

Keywords:

Posted Date: April 22nd, 2021

DOI: https://doi.org/10.21203/rs.3.rs-448939/v1

The carbon economics of vegetative phase change: why plants make juvenile and adult leaves

Authors: Erica H. Lawrence[1], Clint J. Springer[2], Brent R. Helliker[1] and R. Scott Poethig[1]

[1]Department of Biology, University of Pennsylvania, 433 S. University Ave, Philadelphia, Pennsylvania, 19104 USA

[2]Department of Biology, Saint Joseph's University, 5600 City Ave, Philadelphia, Pennsylvania, 19131 USA

Abstract

Across plant species and biomes, a conserved set of leaf traits govern the economic strategy used to assimilate and invest carbon. As plants age, they face new challenges that may require shifts in this leaf economic strategy. In this study, we investigate the role of the developmental transition, vegetative phase change (VPC), in altering carbon economics as plants age. We used overexpression of miR156, the master regulator of VPC, to modulate the timing of VPC in *Populus tremula x alba*, *Arabidopsis thaliana* and *Zea mays* to understand the impact of this transition on leaf economic traits, including construction cost, payback time, and return on investment. Here we find that VPC regulates the shift from a low-cost, quick return juvenile strategy to a high-cost, high-return adult strategy. The juvenile strategy is advantageous in light-limited conditions, whereas the adult strategy provides greater returns in high-light. The transition between these strategies is correlated with the developmental decline in the level of miR156, suggesting that is regulated by the miR156/SPL pathway. Our results provide an eco-physiological explanation for the existence of juvenile and adult leaf types, and suggest that natural selection for these alternative economic strategies could be an important factor in plant evolution.

Introduction

In the plant world carbon is queen. It is the currency with which they build, barter and operate. Plants acquire this resource through the enzymatic reactions of photosynthesis which harnesses light energy from the sun to convert CO_2 into sugars. In order to succeed, plants must photosynthesize efficiently and carbon must be invested wisely.

Leaves are the primary organ through which photosynthesis occurs, and as such, variations in leaf traits that alter carbon economic strategies are of great interest. Leaf construction costs, the amount of carbon required to build leaves, as well as their returns on investment (ROI), determine the resources available for growth and reproduction. Construction cost and ROI are influenced by the morphological and physiological traits that determine leaf chemical composition, photosynthetic capacity (represented by light saturated photosynthetic rate, A_{sat}), respiration (R_d), and leaf lifespan (Poorter, 1994; Poorter *et al.*, 2006). Plants across the globe share conserved relationships between these morphological and physiological traits, creating what is known as the worldwide leaf economics spectrum (LES) (Wright *et al.*, 2004).

The LES uses leaf traits to describe economic strategies ranging from low investment yielding quick returns, to high investment yielding slow returns. Central to the LES is leaf mass per area (LMA), or its inverse specific leaf area (SLA), which describe ratios between leaf area and mass that quantify changes in leaf thickness and density. Often, the high LMA associated with thicker, denser leaves leads to greater proportions of structural tissue that results in a greater construction cost but also longer leaf lifespan (Reich *et al.*, 1992; Poorter *et al.*, 2009). Because of differences in light interception and proportions of photosynthetic tissues, high LMA leaves also tend to have lower mass-based A_{sat}, leading to a high investment, slow-return economic strategy, with the opposite being true for leaves with low LMA (Terashima & Hikosaka, 1995; Reich *et al.*, 1998; Wright *et al.*, 2004; Terashima *et al.*, 2006). Of course, ROI is not directly tied to these strategies as longer lifespan and faster payback of initial cost both have the potential to lead to greater photosynthetic outputs.

While largely ignored, ontogenetic variation in leaf economic strategies is equal in magnitude to that between species (Mason *et al.*, 2013; Hayes *et al.*, 2019; Funk *et al.*, 2020). Shifts in leaf traits from those associated with quick-return to longer-return economic strategies are consistently observed with increasing plant age. Further, trait-trait relationships (i.e. the magnitude with which leaf lifespan increases in response to increasing LMA) are significantly altered across plant development, akin to the alterations induced by environment (Niinemets, 2004; Damián *et al.*, 2018; Liu *et al.*, 2019; Funk *et al.*, 2020). These shifts in leaf traits likely have significant ecological impacts altering plant growth, resource acquisition, and environmental interactions across its lifespan.

Plant ontogeny includes the juvenile-to-adult vegetative transition known as vegetative phase change (VPC). VPC and its master regulator, microRNA156, have been conserved across plant evolution (Axtell & Bowman, 2008). However, the functional significance of this transition, and its impacts on fitness remains a major question in plant developmental biology. As plants progress from the juvenile to adult vegetative phases, the variations in challenges and resources available likely command distinct economic strategies. Previously, we showed that VPC and miR156 modulates morphological and physiological traits central to carbon economics (Lawrence *et al.*, 2020). Specifically, the changes in miR156 expression that drive VPC alter SLA, leaf N and photosynthetic rates across species. miR156-mediated decreases in SLA (equivalent to increases in LMA) between juvenile and adult phases are consistent with the shift from quick to long-return economic strategies previously described. This suggests miR156 is a regulator of ontogenetic changes in leaf carbon economics and that VPC, and the timing of this developmental transition, has important implications for changes in resource use strategies deployed across a plant's lifespan. As a genetically programmed transition, VPC may impact plant fitness by allowing plants to shift between economic strategies as their physiological demands change with age.

In this study we used wildtype and miR156 overexpressor mutants in three diverse species, *Arabidopsis thaliana, Populus tremula x alba,* and *Zea mays,* to investigate how VPC---which is driven by a decline in miR156 expression—is related to ontogenetic shifts in carbon economic strategies. We demonstrate that the previously identified phase-specific changes in leaf morphology and photosynthetic physiology lead to shifts from quick to slow-return economic strategies, and further show that these strategies are likely to be adaptive under different light environments. The evidence that ontogenetic changes in leaf carbon economics are under the regulation of miR156 not only provides a molecular mechanism for this transition in leaf physiology, but also provides an eco-physiological rationale for the existence of vegetative phase change.

Results

Construction cost is higher for adult than juvenile or juvenilized leaves

The chemical composition of adult, juvenile and juvenilized leaves in three test species was determined in order to understand how VPC contributes to leaf construction costs. By using

juvenilized leaves in miR156 overexpressor lines (those with a juvenile phenotype at leaf positions that would normally be adult), we are able separate the effects of VPC from those related to plant size or age. If a measured trait is developmentally phase-specific, juvenilized leaves at "adult" nodes should be more similar to juvenile leaves than to adult leaves. Per gram of leaf tissue, adult, juvenile and juvenilized leaves require the same amount of glucose ($p > 0.05$, Fig. **1A-B**) in *P. tremula x alba* and *A. thaliana*; thus the composition of leaves is similar across development (Table 1). One exception to this similarity was the concentration of nitrate in *A. thaliana* leaves, which was greater in developmentally juvenile leaves ($p < 0.05$). In *Z. mays*, adult leaves have a greater construction cost per gram of tissue than juvenile and juvenilized leaves due to phase-specific differences in carbon, nitrogen, and mineral concentrations ($p < 0.05$) (Fig. **1C**, Table 1).

At the whole leaf level, adult leaves of all three species cost significantly more ($p > 0.05$) glucose to construct than their juvenile and juvenilized counter parts (Fig. **1D-F**). This phase-specific pattern is observed even in *P. tremula x alba* and *A. thaliana* where there are no differences in cost per gram of leaf tissue, due to the significantly greater area and mass of adult leaves compared to both juvenile and juvenilized leaves ($p > 0.05$) (Table S1). Overall, we find that regardless of differences in chemical composition, the effect of VPC on leaf size leads to higher costs for adult compared to juvenile leaves.

Leaf payback time becomes longer as plants transition from juvenile to adult, but the difference in magnitude depends on light environment.

Payback time, the amount of time it takes for a leaf to assimilate the carbon originally invested in its construction, is greater for adult leaves than juvenile or juvenilized leaves across all light levels for all three test species (Fig. **2A-C**). Interestingly, there is a significant interaction between developmental phase and light ($p < 0.05$) in all three species as the difference between developmental phases is greater as light decreases. Specifically, adult leaves of *P. tremula x alba* have, respectively, 7.85 and 3.4 fold longer payback time than juvenile and juvenilized leaves under low-light (10 μmol m^2 s^{-1}), but only 6.6 and 1.79 fold longer payback time under high-light (1000 μmol m^2 s^{-1}). In *A. thaliana,* the payback time for adult leaves is, respectively, 18.8 and 5.7 fold longer under low-light, and 9.4 and 3.16 fold longer under high-light, than for juvenile and juvenilized leaves. Lastly, in *Z. mays*, adult leaves have, respectively,

8.13 and 11.64 fold longer payback time under low-light, and 6.3 and 12 fold longer payback time under high-light than juvenile and juvenilized leaves. Because construction cost remains constant across light levels in our modeled payback time, these differences are a result of photosynthetic responses to light modeled using light response curves (Table **S2**). Similar relationships between payback time and light are observed on a per gram basis for all three species, although to a lesser extent (Fig. **S1**). As we saw with construction costs, the greater similarity between juvenilized leaves with juvenile, as opposed to adult leaves, indicates differences in miR156-mediated development, rather than plant size or age, is responsible for the payback differences observed here.

Leaf lifespan is longer for adult leaves than juvenile leaves

To understand how phase-specific differences in leaf construction cost and payback time impact the overall economic strategy of juvenile and adult leaves, we also measured the photosynthetic lifespan of these leaves. Previously, we determined that SLA, which is closely connected to lifespan, is a phase-specific trait, with adult leaves having lower SLA (or higher LMA) compared to both juvenile and juvenilized leaves of all three test species (Table S1, Lawrence *et al.*, 2020b). Across species, thicker, more dense adult leaves (low SLA) had significantly longer ($p < 0.05$) lifespans than juvenile leaves (Fig. **2D-F**). Lifespan differences between juvenile and adult leaves ranged from 26 and 23 days in *P. tremula x alba* and *Z. mays,* respectively, to 8 days in *A. thaliana*. Of note, the low-light payback time for adult *Z. mays* leaves (which approaches 52 days) far exceeds the 34-day average lifespan of these leaves.

Light environment alters the phase-specific relationship of leaf return on investment

Despite higher construction cost and longer payback time, lifespan differences produce a higher return on investment (ROI) for adult leaves than for juvenile leaves, across most light environments (Fig. **2G-I**). Adult leaves outperform juvenile leaves in high-light environments (1000 μmol m^2 s^{-1}) with 14, 2.8 and 18 times more glucose returns for *P.tremula x alba*, *A. thaliana* and *Z. mays* respectively. However, in low-light environments (10 μmol m^2 s^{-1}), adult leaves experience net carbon loss with 4.3, 4.6 and 5.1 times fewer returns than juvenile leaves. Furthermore, the ROI for juvenile leaves is less sensitive to light environment than is the case for adult leaves. Juvenile leaves approach their maximum ROI at a PPFD around 10 mol m^{-2} day^{-1}

whereas, with the exception of *A. thaliana*, which was grown under low-light conditions for this experiment, the ROI for adult leaves continues to increase as PPFD increases, well past 40 mol m^{-2} day^{-1}. ROI per gram of tissue display similar patterns across light environments to leaf-based measures in *P. tremula x alba* and *Z. mays.* However, in *A. thaliana,* juvenile tissue maintains a higher ROI than adult tissue across all light environments (Fig. **S1**).

Photosynthetic induction is faster in juvenile leaves than in adult leaves

Because light levels continuously fluctuate throughout the day in forests and crop fields (i.e. from the sun moving across the sky, leaves fluttering in the wind, etc.), modeling carbon economics of *P. tremula x alba* and *Z. mays* under more realistic conditions required an analysis of the rate of photosynthetic induction in juvenile and adult leaves. Upon exposure to saturating light, juvenile leaves of both species more quickly reached higher photosynthetic rates and induction states than adult leaves (Fig. **3**). The relaxation times for Rubisco activation were not significantly different ($p < 0.05$) between juvenile and adult leaves (Table S3), indicating that developmental differences in induction occur prior to 1 min, during the 'fast-phase' of induction.

Alternatively, developmental differences in induction could be due to a combination of traits, such as stomatal conductance and Calvin cycle intermediate accumulation, rather than solely to the activation of Rubsico. In *P. tremula x alba,* differences in photosynthetic induction are apparent by 1 min of high-light exposure, suggesting phase-specific differences in induction are likely present before exposure to high-light, or during the first minute, when buildup of intermediates in the Calvin cycle are most important. This is not the case for *Z. mays,* where juvenile leaves reach a higher induction state than adult leaves during this 'slow-phase' period of minutes 1-10 (Fig. **3D**). These results suggest that while juvenile leaves of both species have faster photosynthetic induction properties than their adult counter parts, the mechanisms behind these differences may vary between species.

Dynamic light models show phase-specific leaf economic relationships are more dependent on daily light than number of sunflecks

For both *P. tremula x alba* and *Z. mays,* the dynamics of light environment had a significant effect ($p < 0.05$) on the relationship of payback time and ROI between juvenile and adult leaves (Fig. **4A,C**, Fig. **5A,C**). Over 156 different light simulations, daily PPFD varied

between 18 and 32 mol m^{-2} day^{-1} while the number of sunflecks varied between 1 and 242 (figures of simulated light environments in Fig. **S2**). The carbon economic traits of adult leaves were much more affected by PPFD compared to juvenile leaves, as indicated by the smaller slope of the negative relationship with payback time, and the larger slope of the positive relationship with ROI for adult leaves of both species (Table S4). Similar trends are observed on a per gram of tissue basis, although differences between juvenile and adult leaf payback time across PPFD are not significant ($p > 0.05$) for *P. tremula x alba* (Fig. **S3**, Table S4).

Surprisingly, there was no significant interaction between developmental phase and number of sunflecks for payback time or ROI in *P. tremula x alba* (Fig. **4B,D**)(Table S4). While significant interactions ($p < 0.05$) were present for these relationships in *Z. mays*, the low R^2 values for both developmental phases and economic traits ($R^2 \leq 0.05$), indicate that sunflecks have a minor effect on payback time and ROI (Table S4). There were no significant differences in the way juvenile and adult tissue responded to sunflecks on a per gram basis, and any significant relationships between payback time or ROI and sunflecks for either developmental stage was minor ($R^2 \leq 0.05$) (Fig. **S3, S4**, Table S4).

Despite there being no meaningful relationship between carbon economics and number of sunflecks, lags in photosynthetic response to light fluctuations due to the rate of induction resulted in assimilation loss for both developmental phases in both species. As the number of sunflecks increased and plants were exposed to more rapid changes in light, the assimilation lost due to a lag in induction also increased (Fig. **6**). In both species, the faster induction rate in juvenile leaves resulted in lower assimilation losses compared to adult leaves ($p < 0.05$). Nevertheless, the impact of these losses on carbon economics in these simulated environments is minimal compared to the effect of overall changes in PPFD.

Discussion

Vegetative phase change alters plant economic strategies through miR156-mediated changes in leaf morphology and physiology. Juvenile leaves— which have high levels of miR156— use a low-cost, quick-return economic strategy, whereas adult leaves— which have low levels of miR156— use a high-cost, slow-return strategy. The adult strategy carries more risk than the juvenile strategy, but has the potential to provide high ROI (Fig. **7)**. This developmental shift in strategy is brought about by the same traits that govern leaf economics

across species and environments in the LES, namely leaf lifespan and LMA (Wright *et al.*, 2004). Across species, adult leaves have high LMA and long lifespan while juvenile leaves have low LMA and shorter lifespan (Fig. **2D-F**, Table S1). In *Z. mays,* leaf N and the photosynthetic rates of juvenile and adult leaves follow the established trait relationships within the LES as the low LMA juvenile leaves also have higher mass-based measures of N and A_{sat} compared to adult leaves (Table 1, Lawrence *et al.*, 2020b). As previously reported, trait-trait relationships of the LES are not always conserved at smaller than global scales (Edwards *et al.*, 2014; Mason & Donovan, 2015b; Anderegg *et al.*, 2018). We find this to be the case for developmental changes in leaf N and A_{sat} in *P. tremula x alba* and *A. thaliana,* as these leaves have no significant differences in mass-based measures of N and A_{sat} despite their differences in LMA. It is unclear why the expected negative relationships between LMA and leaf N or A_{sat} are lacking, as LMA increases during VPC in these species. However, previous work found no phase-specific changes in photosynthetic nitrogen use efficiency (PNUE) (Lawrence *et al.*, 2020), indicating adult leaves somehow compensate for the structural changes that often reduce PNUE in high LMA leaves, potentially through their increased stomatal density which could reduce resistance to CO_2 diffusion (Hikosaka, 2004; Feng *et al.*, 2016; Lawrence *et al.*, 2021).

These developmentally programmed changes in leaf carbon economic strategy are likely to have ecological implications because plants face different biotic and abiotic challenges during their lifetime. For example, juvenile leaves, which have a photosynthetic advantage over adult leaves under low-light (Lawrence *et al.*, 2020), are more likely to be found in low, highly dynamic, light environments because young plants are often shaded by their neighbors, and quickly self-shade due to their relatively rapid rate of leaf production (Wang *et al.*, 2008). Here we find that the economic strategy of juvenile leaves further adds to this low-light advantage as these leaves are able to maintain a positive carbon balance even at very low light levels (Fig. **2, 7**). The payback time of adult leaves dramatically increases under low-light, greatly reducing ROI and, in some cases, exceeds the lifespan of a leaf, resulting in net carbon loss. On the other hand, the magnitude with which adult ROI exceeds that of juvenile leaves increases significantly with increasing irradiance (Fig. **2**). Overall, the economic strategy of juvenile leaves appears to be less sensitive to light environment, making it a low-risk, low-reward strategy that is likely beneficial for a young plant with minimal carbon reserves. Although the high-cost strategy of

adult leaves incurs greater risk because of long-term environmental variability, the high-reward potential of this strategy may outweigh this risk.

Surprisingly, the ability of juvenile leaves to respond more quickly to sunflecks than adult leaves had little effect on the carbon economic relationships between these leaves in our dynamic light models (Fig. **4,5**). In our simulated environments, we held the total time leaves were exposed to sunflecks relatively constant but allowed the number of sunflecks to vary dramatically. As a result, there was no correlation between the number of sunflecks and daily integrated PPFD. It may be that developmental differences in induction rate have a greater influence on carbon economic relationships when sunflecks play a large role in determining daily PPFD, such as in a rainforest understory where sunflecks can account for 52% of daily light (Chazdon & Pearcy, 1991).

The developmental differences in carbon economics described here indicate that genotypic variation in miR156 expression, and subsequently the timing of VPC, could have significant consequences for plant ecology and evolution. Among other things, leaf economic strategies alter plant growth and survival in response to nutrient and water availability, herbivory, competition and light environment (Coley, 1988; Poorter *et al.*, 2006; Reich, 2014; Mason & Donovan, 2015a; Russo & Kitajima, 2016; Adams *et al.*, 2020). That the developmentally regulated changes in leaf economic strategy are conserved among juvenile and adult leaves of three phylogenetically diverse species, and that this strategy confers the ability to respond to changes in environmental factors, suggests these ontogenetic changes in carbon economics are widely advantageous. A better understanding of natural variation in the timing of VPC, and the function of this process in plant physiology and response to environmental stressors, is crucial for determining the role of this developmental transition in plant ecology and evolution.

Materials and Methods

Plant Material

Populus tremula x alba line 717-1B4 and miR156 overexpressor line 40 described in Lawrence *et al.*, (2021) were obtained by *in vitro* propagation and hardened on propagation media as described in Meilan & Ma (2006). Plants were then transplanted to Fafard-2 growing mix (Sun Gro Horticulture, Massachusetts, USA) in 0.3-L pots in the greenhouse at the

University of Pennsylvania (39.9493°N, 75.1995°W, 22.38 m a.s.l.) and kept in plastic bags for increased humidity for 2 weeks. Plants were transferred to 4.2-L pots with Fafard-52 growing mix 3 weeks later and fertilized with Osmocote 14-14-14 (The Scotts Company, Marysville, OH, USA). Plants were additionally fertilized once a week with Peters 20-10-20 (ICL Fertilizers, Dublin, OH, USA). Greenhouse conditions consisted of a 16-hr photoperiod with temperatures between 22 and 27°C. Light levels were based on natural light and supplemented with 400-W metal halide lamps (P.L. Light Systems, Ontario, Canada) with daily irradiances between 300 to 1,500 μmol m^{-2} s^{-1} across the day. All settings controlled by Priva (Ontario, Canada) and Microgrow (Temecula, Canada) greenhouse systems.

Z. mays seeds with the *Corngrass 1 (Cg1)* mutation (stock 310D)—which consists of a tandem duplication of miR156b/c primary sequences described in Chuck et al. (2007)— and the W22 inbred line were obtained from the Maize Genetics Cooperation Stock Center (Urbana, IL, USA). Plants heterozygous for *Cg1* were crossed to W22 to produce the *Cg1/+ and +/+* siblings used in this study. Seeds were planted in 9.09-L pots with Fafard-52 growing mix and fertilized with Osmocote 14-14-14 in the greenhouse under growing conditions described above.

A. thaliana (Col) and the 35S:miR156 overexpressor line described in Wu & Poethig (2006) were planted in 0.06-L pots with Fafard-2 growing mix. Beneficial nematodes (*Steinernema feltiae*, BioLogic, Willow Hill, PA), Marathon→ 1% granular insecticide and diatomaceous earth were added to the growing mix to control insects. Planted seeds were placed at 4°C for 3 days before being grown at 22°C in Conviron growth chambers (Pembina, ND, USA) under short days (10 hrs. light/14 hrs. dark) at 60 μmol m^{-2} s^{-1} light to obtain leaves large enough to fit in the gas exchange chamber. Plants were fertilized with Peters 20-10-20 every other week.

Individuals from genotypes of all species were positioned in a randomized fashion and rotated frequently. Planting was staggered across two, three and five months for *Arabidopsis, P. tremula x alba* and *Z. mays* respectively.

Leaf samples

All samples were taken from the uppermost fully expanded leaf. For all three species, naturally juvenile and adult leaves in wild-type lines and "juvenilized" leaves, those in miR156 overexpressor lines with a juvenile phenotype at leaf positions that would normally be adult,

were sampled. In *P. tremula x alba,* developmental stage was determined by petiole shape and abaxial trichome density as described in Lawrence *et al.*, (2021). Juvenile leaves were sampled from wild-type node 10 and adult from node 25, and juvenilized leaves were sampled from overexpressor node 25. In *Z. mays*, developmental stage was determined by the presence or absence of epicuticular wax and trichomes as described in Poethig (1988). Juvenile leaves were sampled from node 4 and adult from node 11 in wildtype plants, and juvenilized leaves sampled from node 4 in *Cg1* mutants. In *A. thaliana,* developmental stage was determined by the presence or absence of abaxial trichomes. Juvenile leaves were sampled from node 5 for physiological and morphological measurements and nodes 2-5 for construction cost measures, and adult and juvenilized from node 10 and 10-15 in wildtype and miR156 overexpressors, respectively.

Leaf Construction Cost Determination

Area of fresh leaf samples was determined from photographs using FIJI software (Schindelin *et al.*, 2012). Samples were then dried at 60°C until consistent mass, ground using a Willey Mill until small enough to pass through a 2 mm grinding mesh, and then ground further using a mortar and pestle. Each *Z. mays* sample consisted of ~100 mg tissue from one leaf, *P. tremula x alba* samples consisted of ~100-120 mg tissue from between 1 and 4 leaves, and *A. thaliana* samples consisted of ~60-80 mg tissue from around 60 leaves. Chemical composition analysis was performed as described in Cataldo *et al.*, (1975), Poorter, (1994), and Poorter & Villar, (1997).

1 mg from each sample was used to determine C and N using an ECS 4010 CHNSO Analyzer (Costech Analytical Technologies INC, Valencia, CA, USA).

For nitrate determination, 20 mg of sample was added to 2 ml 80°C water for 20 mins for nitrate extraction. Samples were centrifuged at 5000 rcf for 15 mins. 0.2 ml of supernatant was mixed with 0.8 ml of 5% (w/v) salicylic acid in H_2SO_4 and incubated at room temperature for 20 mins. Following incubation, 19 ml of 2N NaOH was added to samples. Absorbance of 410 nm was determined for 0.2 ml aliquots of each sample and NO^-_3-N standards of 1 to 200 µg, used to create a standard curve.

The remaining tissue was weighed and used for mineral determination. Samples were ashed at 550°C in a muffle furnace for 6 hrs and weighed again. Ash alkalinity was determined in duplicate for each sample to measure CO_3^{-2} that formed when oxides from the plant tissue

reacted with CO_2 upon cooling. 4 mg of ash was mixed in 5 mL of deionized H_2O and 2-3 drops of 0.5% phenolphthalein were added. The solution was titrated with 0.5N HCl until the pink indicator color disappeared. An additional volume of HCl, equal to that needed for titration plus an additional 2 mL, was added to the sample. The solution was then boiled for 5 mins, cooled to room temperature and an additional 2-3 drops of phenolphthalein were added. Samples were then back titrated with 0.5N NaOH until a faint pink color persisted. The average alkalinity from the two replicates of each sample was used in calculations.

All equations for calculations are presented in the appendix. Ash alkalinity was calculated using equation (1.1), mineral content equation (1.2), and construction cost of leaf tissue in grams of glucose using equation (1.3). Tissue mass lost in this process was assumed to have the same chemical composition as that recovered.

Photosynthetic Measurements

All gas exchange measurements were made using a Li-6400 portable photosynthesis machine (Li-Cor Environmental, Lincoln, NE, USA) at a leaf temperature of 25°C following acclimatization to starting chamber conditions. Light response curves were performed in all three species at a reference [CO_2] of 400 ppm using a minimum wait time of 2 mins between light level changes and data logging. Net photosynthetic rate (A_{net}) in *A. thaliana* was measured at light levels of 1000, 800, 600, 300, 200, 150, 100, 75, 50, 25, 0 µmol m^{-2} s^{-1} at a flow rate of 300 µmol air sec^{-1}, in *Zea mays* at light levels of 1800, 1500, 1200, 1000, 800, 600, 300, 200, 150, 100, 75, 50, 25, 0 µmol m^{-2} s^{-1} at a flow rate of 400 µmol air sec^{-1}, and *P. tremula x alba* at light levels of 1500, 1200, 1000, 800, 600, 300, 200, 150, 100, 75, 50, 25, 10 and 0 µmol m^{-2} s^{-1} at a flow rate of 400 µmol air sec^{-1}.Light response curves were analyzed using the {AQ Curve fitting} script in R (Tomeo, 2019) which uses equations based on a standard non-rectangular hyperbola model fit described in Lobo et al. (2013) and found in the appendix as equation (2.1).

Photosynthetic induction was measured on leaves exposed to light levels less than 20 µmol m^{-2} s^{-1} for a minimum of 20 mins. Induction was measured by logging every 10 seconds as leaves were exposed to 20 µmol m^{-2} $s^{-1}$of light for 2 mins and then shifted to saturating light, 1800 µmol m^{-2} s^{-1} for *P. tremula x alba* and *Z. mays* or 1000 µmol m^{-2} s^{-1} for *A. thaliana*, for 20 mins.

Carbon Economics Calculations

All equations for calculations are described in Poorter, (1994) and Poorter *et al.*, (2006) and presented in the appendix. Assimilation and respiration rates were converted from μmol CO_2 m^{-2} to grams of glucose per gram of tissue using equation (3.1). Specific leaf area (SLA) used in this equation was calculated by dividing the fresh leaf area by its dry weight. Payback time, the time in days required for leaves to assimilate the equivalent glucose needed to construct it, was determined using equation (4.1). Return on investment (ROI) was calculated using equation (4.2). Leaf lifespan represents the photosynthetic lifespan measured as the time between full expansion and senescence, determined by the first signs of discoloration. Payback time and ROI calculations were based on days with 12 hr day/night cycles. Assimilation was modeled using equation (2.1) with the light response curve parameters previously determined. Respiration (R_d) used in these equations was estimated as 7% A_{sat} to minimize measurement errors that may arise when measuring low gas exchange rates with portable photosynthesis machines as suggested in Poorter *et al.*, (2006). For calculations of payback time and ROI in constant light environments, integrated daily photon flux density (PPFD) was calculated using equation (5.1).

Dynamic Light Environment Model

All parts of the dynamic light environment model were written in R (R Core Team, 2018) and provided as RMarkdown files in the supplement of this manuscript. All equations used are provided in the appendix.

Part 1 of the model determines light levels across the day based on Campbell & Norman, (1998), Zhu *et al.*, (2004) and Salter *et al.*, (2019). Solar declination angle (eq. 6.1), hour angle (eq. 6.2), and solar elevation angle (eq. 6.3) were calculated using a latitude of Philadelphia, PA, USA (39.95°N or 0.697 rads) and Julian day of 180. Direct and diffuse light were calculated using equations (6.4) and (6.5) respectively. Solar constant was assumed to be 2600 μmol m^{-2} s^{-1} and atmospheric transmissivity 0.75. Light levels during sun and shade flecks were determined using equations (6.6) and (6.7) respectively. Leaf area index (LAI) varied between 0.5 and 8 for each simulation and are reported in Table **S5**.

Part 2 of the model determines when light switches between sun and shadeflecks using equations (7.1) and (7.2) described in Salter *et al.*, (2019). Day light began at 6:00 and ended at

18:00 with simulations set to begin with a sunfleck. Initial sunfleck lengths varied between simulations and are reported Table **S5**.

Part 3 of the model determines assimilation across the day using variables from the light response curves and photosynthetic induction measurements based on Woodrow & Mott, (1989), Mott & Woodrow, (2000), and Taylor & Long, (2017). To determine tau, which describes Rubisco kinetics for photosynthetic induction, A_{sat} and instantaneous net photosynthetic rate (A_{net}) during induction were corrected for changes in intercellular [CO_2] (C_i) using equations (8.1) and (8.2) respectively. C_i corrected measures of A_{sat} are referred to as A_f^* and A_{net} as A^*. Tau during increases in light was then calculated as the inverse of the linear slope of $ln(A_f^*-A^*)$ vs Time for minutes 1-10 of induction upon exposure to high-light (eq. 8.3). The initial minute of induction, often referred to as the 'fast phase', was excluded from our model because 1) increases in A_{net} during this phase are primarily governed by increases in the pool of RuBP and therefore, Rubsico kinetics cannot accurately be estimated using gas exchange, and 2) at times greater than 1 min, which is the resolution of our model, the contribution of this phase to A_{net} is negligible and can be excluded (Woodrow & Mott, 1989). At times greater than 10 mins, most changes in A_{net} are governed by stomatal opening, and therefore A^* shows little change (Woodrow & Mott, 1989). Tau during decreases in light describes the deactivation of Rubisco. Because A_{net} decreases more quickly than Rubisco deactivation when light levels are reduced, tau during deactivation is difficult to estimate using gas exchange. Woodrow & Mott, (1989) showed that when measured biochemically, tau during deactivation was roughly 5x tau during induction, we therefore estimated our values in this way. Induction state, representing the percent of A_{sat} instantaneous assimilation is at during induction was calculated by equation (8.4).

A_{net} throughout the day required the calculation of the potential maximum assimilation rate (A_f, eq. 9.1) and initial assimilation rate prior to induction (A_i, eq. 9.2) for each 1 min interval as described in Woodrow & Mott, (1989) and Taylor & Long, (2017). Tau, A_f and A_i were then used in equation (9.3), as described in Mott & Woodrow, (2000), to calculate A_{net} for each time point. Integrated assimilation (A_{int}) across each modeled 1 min interval was calculated by equation (9.4). To estimate the loss in assimilation due to lags in the response of photosynthesis to light, A_{int} with a square response to each change in light was calculated by setting tau equal to 0 in equation (9.4). Subtracting A_{int} with induction responses (tau = slope of

431 $ln(A_f^*-A^*)$ vs Time) from A_{int} with immediate square responses to light (tau = 0) provides the
432 loss in assimilation due to Rubisco activation.
433 Part 4 of the model uses the same equations described above to calculate payback time
434 and ROI for each simulation. For all modeled calculations, median values for each species and
435 developmental stage were used for assimilation variables and mean values for construction cost
436 and leaf trait variables.
437
438 *Statistical Analysis*
439 All statistical analyses were performed in JMP® Pro v. 14.0.0 (SAS Institute Inc., Cary,
440 NC). Leaf composition, leaf morphology, construction cost, and light response curve parameters
441 between adult, juvenile and juvenilized leaves of each species were compared by one-way
442 ANOVA, where developmental stage was the main effect. When ANOVA results were
443 significant ($p < 0.05$), a Student's *t* test was performed to determine differences between
444 developmental groups. Traits were considered to be affected by developmental phase when adult
445 leaves were significantly different from both juvenile and juvenilized leaves with the same trend.
446 Light induction parameters and leaf lifespan of juvenile and adult leaves of each species were
447 compared using a Student's *t* test and considered significantly different when $p < 0.05$. Payback
448 time, ROI, photosynthetic rate during induction, induction state, and lost assimilation due to slow
449 induction for each species were compared by ANCOVA with developmental stage as the
450 covariate and considered significantly different when $p < 0.05$.
451
452
453 **Acknowledgements**
454 We thank Samara Gray and Joshua Darfler for their assistance in caring for the plants
455 used in this study. This research was funded by the NSF Graduate Research Fellowship
456 (Division of Graduate Education; DGE-1845298), U. of Pennsylvania SAS Dissertation
457 Research Fellowship and the Peachey Research Fund awarded to E.H.L. and NIH GM51893
458 awarded to R.S.P.
459
460 **References**
461 **Adams HD, Felton AJ, Fajardo A, Cheng D, Chen X, Sun J, Wang M, Lyu M, Niklas KJ,**

Michaletz ST, *et al.* 2020. The leaf economics spectrum constrains phenotypic plasticity across a light gradient. *Frontiers in Plant Science* **11**: 735.

Anderegg LDL, Berner LT, Badgley G, Sethi ML, Law BE, HilleRisLambers J. **2018**. Within-species patterns challenge our understanding of the leaf economics spectrum. *Ecology Letters* **21**: 734–744.

Axtell MJ, Bowman JL. **2008**. Evolution of plant microRNAs and their targets. *Trends in Plant Science* **13**: 343–349.

Campbell GS, Norman JM. **1998**. *An Introduction to Environmental Biophysics*. New York: Springer Verlag.

Cataldo DA, Haroon MH, Schrader LE, Youngs VL. **1975**. Rapid colorimetric determination of nitrate in plant tissue by nitration of salicylic acid. *Communications in Soil Science and Plant Analysis* **6**: 71–80.

Chazdon RL, Pearcy RW. **1991**. The Importance of Sunflecks for Forest Understory Plants. *BioScience* **41**: 760–766.

Chuck G, Cigan M, Saeteurn K, Hake S. **2007**. The heterochronic maize mutant *Corngrass1* results from overexpression of a tandem microRNA. *Nature genetics* **39**: 544–549.

Coley PD. **1988**. Effects of plant growth rate and leaf lifetime on the amount and type of anti-herbivore defense. *Oecologia* **74**: 531–536.

Damián X, Fornoni J, Domínguez CA, Boege K. **2018**. Ontogenetic changes in the phenotypic integration and modularity of leaf functional traits. *Functional Ecology* **32**: 234–246.

Edwards EJ, Chatelet DS, Sack L, Donoghue MJ. **2014**. Leaf life span and the leaf economic spectrum in the context of whole plant architecture (W Cornwell, Ed.). *Journal of Ecology* **102**: 328–336.

Feng S, Xu Y, Guo C, Zheng J, Zhou B, Zhang Y, Ding Y, Zhang L, Zhu Z, Wang H, *et al.* 2016. Modulation of miR156 to identify traits associated with vegetative phase change in tobacco *(Nicotiana tabacum*). *Journal of Experimental Botany* **67**: 1493–1504.

Funk JL, Larson JE, Vose G. **2020**. Leaf traits and performance vary with plant age and water availability in *Artemisia californica*. *Annals of Botany* **3**: 1–9.

Hayes FJ, Buchanan SW, Coleman B, Gordon AM, Reich PB, Thevathasan N V, Wright IJ, Martin AR. **2019**. Intraspecific variation in soy across the leaf economics spectrum. *Annals of Botany* **123**: 107–120.

Hikosaka K. **2004**. Interspecific difference in the photosynthesis-nitrogen relationship: Patterns, physiological causes, and ecological importance. *Journal of Plant Research* **117**: 481–494.

Lawrence EH, Leichty AR, Doody EE, Ma C, Strauss SH, Poethig RS. **2021**. Vegetative phase change in *Populus tremula x alba*. *New Phytologist*: nph.17316.

Lawrence EH, Springer CJ, Helliker BR, Poethig RS. **2020**. MicroRNA156-mediated changes in leaf composition lead to altered photosynthetic traits during vegetative phase change. *New Phytologist*: nph.17007.

Liu Z, Jiang F, Li F, Jin G. **2019**. Coordination of intra and inter-species leaf traits according to leaf phenology and plant age for three temperate broadleaf species with different shade tolerances. *Forest Ecology and Management* **434**: 63–75.

Lobo F de A, de Barros MP, Dalmagro HJ, Dalmolin ÂC, Pereira WE, de Souza ÉC, Vourlitis GL, Rodríguez Ortíz CE. **2013**. Fitting net photosynthetic light-response curves with Microsoft Excel - a critical look at the models. *Photosynthetica* **51**: 445–456.

Mason CM, Donovan LA. **2015a**. Does investment in leaf defenses drive changes in leaf economic strategy? A focus on whole-plant ontogeny. *Oecologia* **177**: 1053–1066.

Mason CM, Donovan LA. **2015b**. Evolution of the leaf economics spectrum in herbs: Evidence from environmental divergences in leaf physiology across *Helianthus* (*Asteraceae*). *Evolution* **69**: 2705–2720.

Mason CM, Mcgaughey SE, Donovan LA. **2013**. Ontogeny strongly and differentially alters leaf economic and other key traits in three diverse *Helianthus* species. *Journal of Experimental Botany* **64**: 4089–4099.

Meilan R, Ma C. **2006**. Poplar (*Populus* spp.). In: Wang K, ed. Methods in Molecular Biology: Agrobacterium Protocols. Totowa, NJ: Humana Press Inc., 143–151.

Mott KA, Woodrow IE. **2000**. Modelling the role of Rubisco activase in limiting non-steady-state photosynthesis. *Journal of Experimental Botany* **51**: 399–406.

Niinemets Ü. **2004**. Adaptive adjustments to light in foliage and whole-plant characteristics depend on relative age in the perennial herb *Leontodon hispidus*. *New Phytologist* **162**: 683–696.

Poethig RS. **1988**. Heterochronic mutations affecting shoot development in maize. *Genetics* **119**: 959–73.

Poorter H. **1994**. Construction costs and payback time of biomass: A whole plant perspective. In: J. Roy and E. Garnier, ed. A Whole Plant Perspective on Carbon-Nitrogen Interactions. The

Netherlands: SPB Academic Publishing, 111–127.
Poorter H, Niinemets Ü, Poorter L, Wright IJ, Villar R. **2009**. Causes and consequences of variation in leaf mass per area (LMA): a meta-analysis. *New Phytologist* **182**: 565–588.
Poorter H, Pepin S, Rijkers T, De Jong Y, Evans JR, Kö Rner C. **2006**. Construction costs, chemical composition and payback time of high-and low-irradiance leaves. *Journal of Experimental Botany* **57**: 355–371.
Poorter H, Villar R. **1997**. The Fate of Acquired Carbon in Plants: Chemical Composition and Construction Costs. In: Bazzaz FA, Grace J, eds. Plant Resource Allocation. New York: Academic Press, 39–72.
Reich PB. **2014**. The world-wide 'fast-slow' plant economics spectrum: A traits manifesto. *Journal of Ecology* **102**: 275–301.
Reich PB, Ellsworth DS, Walters MB. **1998**. Leaf structure (specific leaf area) modulates photosynthesis–nitrogen relations: evidence from within and across species and functional groups. *Functional Ecology* **12**: 948–958.
Reich PB, Walters MB, Ellsworth DS. **1992**. Leaf Life-Span in Relation to Leaf, Plant, and Stand Characteristics among Diverse Ecosystems. *Ecological Monographs* **62**: 365–392.
Russo SE, Kitajima K. **2016**. The Ecophysiology of Leaf Lifespan in Tropical Forests: Adaptive and Plastic Responses to Environmental Heterogeneity. In: Goldstein G, Santiago LS, eds. Tropical Tree Physiology. Switzerland: Springer International Publishing, 357–383.
Salter WT, Merchant AM, Richards RA, Trethowan R, Buckley TN. **2019**. Rate of photosynthetic induction in fluctuating light varies widely among genotypes of wheat. *Journal of Experimental Botany* **70**: 2787–2796.
Schindelin J, Arganda-Carreras I, Frise E, Kaynig V, Longair M, Pietzsch T, Preibisch S, Rueden C, Saalfeld S, Schmid B, *et al.* 2012. Fiji: An open-source platform for biological-image analysis. *Nature Methods* **9**: 676–682.
Taylor SH, Long SP. **2017**. Slow induction of photosynthesis on shade to sun transitions in wheat may cost at least 21% of productivity. *Philosophical Transactions of the Royal Society B* **372**: 20160543.
Terashima I, Hanba YT, Tazoe Y, Vyas P, Yano S. **2006**. Irradiance and phenotype: Comparative eco-development of sun and shade leaves in relation to photosynthetic CO2 diffusion. *Journal of Experimental Botany* **57**: 343–354.

Terashima I, Hikosaka K. **1995**. Comparative ecophysiology of leaf and canopy photosynthesis. *Plant, Cell & Environment* **18**: 1111–1128.

Tomeo N. **2019**. Tomeopaste/AQ_curves: AQ_curve fitting release 1. doi.org/10.5281/zenodo.3497557.

Wang JW, Schwab R, Czech B, Mica E, Weigel D. **2008**. Dual effects of miR156-targeted SPL genes and CYP78A5/KLUH on plastochron length and organ size in *Arabidopsis thaliana*. *Plant Cell* **20**: 1231–1243.

Woodrow IE, Mott KA. **1989**. Rate limitation of non-steady-state photosynthesis by ribulose-1,5-bisphosphate carboxylase in spinach. *Australian Journal of Plant Physiology* **16**: 487–500.

Wright IJ, Reich PB, Westoby M, Ackerly DD, Baruch Z, Bongers F, Cavender-Bares J, Chapin T, Cornelissen JHC, Diemer M, *et al.* 2004. The worldwide leaf economics spectrum. *Nature* **428**: 821–827.

Wu G, Poethig RS. **2006**. Temporal regulation of shoot development in *Arabidopsis thaliana* by miR156 and its target SPL3. *Development* **133**: 3539–3547.

Zhu X-G, Ort DR, Whitmarsh J, Long SP. **2004**. The slow reversibility of photosystem II thermal energy dissipation on transfer from high to low light may cause large losses in carbon gain by crop canopies: a theoretical analysis. *Journal of Experimental Botany* **55**: 1167–1175.

574

575 **Table 1.** Leaf composition of adult, juvenile and juvenilized leaves of *P. tremula x alba, A*
576 *thaliana* and *Z. mays*. Values indicate the mean ± standard error. For traits where ANOVA
577 results were significant ($p < 0.05$), lower case letters indicate significant ($p < 0.05$) differences
578 between developmental groups determined by a Student's *t* test.

Species	Development	Carbon (mg g^{-1})	Nitrogen (mg g^{-1})	Nitrate (mg g^{-1})	Mineral (mg g^{-1})	n
P. tremula x alba	Adult	793.96 ± 29.96	37.06 ± 2.24	0.14 ± 0.03^{b}	168.97 ± 30.86^{b}	5
	Juvenile	730.22 ± 69.20	63.22 ± 11.25	0.31 ± 0.10^{a}	206.56 ± 59.56^{b}	4
	Juvenilized	618.49 ± 72.95	72.92 ± 17.19	0.21 ± 0.04^{b}	308.58 ± 59.60^{a}	5
A. thaliana	Adult	547.87 ± 72.32	106.03 ± 28.01	2.10 ± 0.39^{b}	346.1 ± 69.95	3
	Juvenile	564.59 ± 10.70	98.11 ± 27.55	2.58 ± 0.24^{a}	337.29 ± 37.08	3
	Juvenilized	536.19 ± 22.86	123.82 ± 7.97	2.46 ± 0.21^{a}	339.98 ± 30.77	3
Z. mays	Adult	772.74 ± 5.21^{a}	24.73 ± 3.43^{b}	0.09 ± 0.01^{b}	202.52 ± 3.26^{c}	5
	Juvenile	620.09 ± 5.69^{b}	42.86 ± 4.82^{a}	0.30 ± 0.04^{a}	337.05 ± 8.44^{a}	5
	Juvenilized	687.2 ± 14.14^{c}	43.77 ± 1.33^{a}	0.17 ± 0.02^{b}	269.03 ± 14.00^{b}	5

579
580

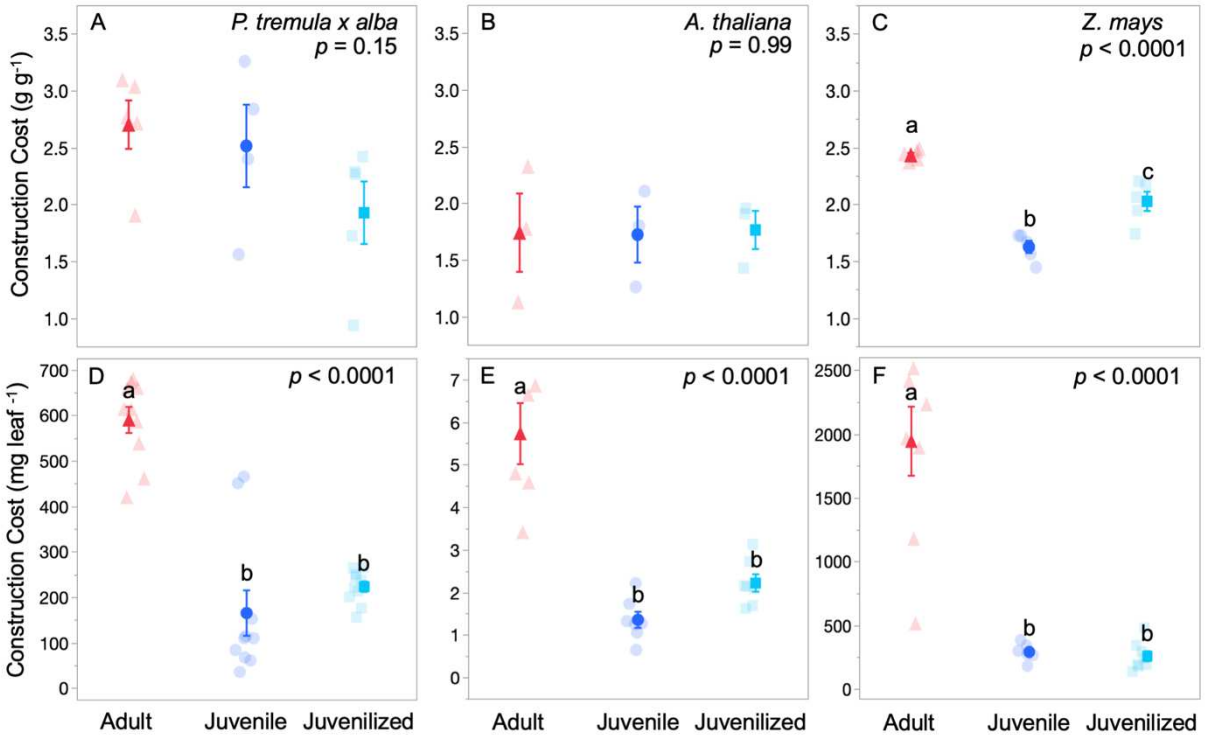

Figure 1. Construction cost in grams of glucose per gram of leaf tissue (A-C) or per leaf (D-F) for adult (red triangles), Juvenile (blue circles), and juvenilized (light blue squares) leaves of *P. tremula x alba* (A, D), *A. thaliana* (B, E), and *Z. mays* (C-F). Data presented as means ± s.e.m. by solid symbols and individual replicates by transparent symbols. *P*-values determined by one-way *ANOVA* with leaf development as the effect. Different lower-case letters represent groups significantly different from each other as determined by Student's *T*.

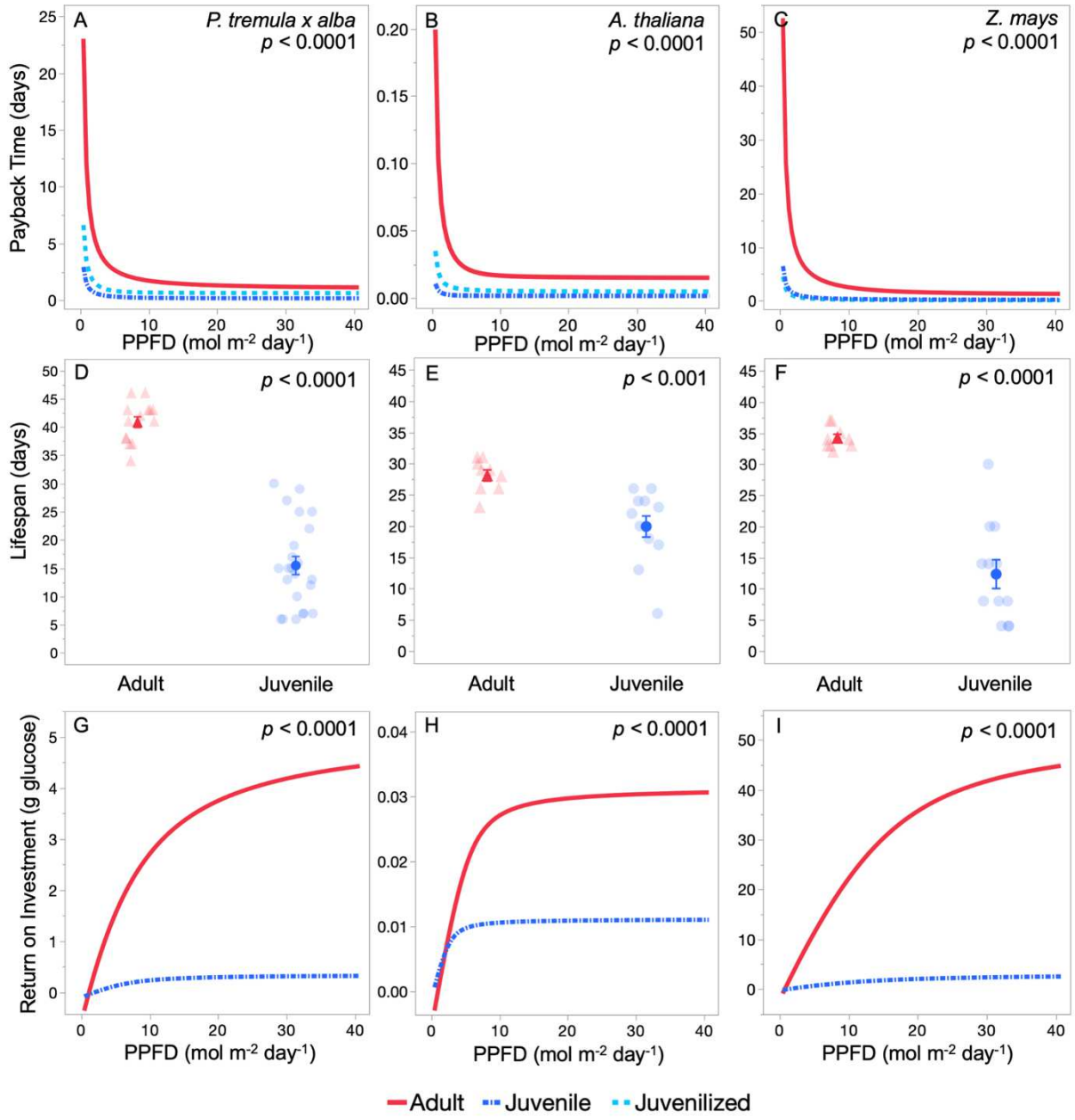

Figure 2. Payback time per leaf (A-C), leaf lifespan (D-F) and return on investment (ROI) per leaf in grams of glucose (G-I) for adult (red triangles and solid lines), juvenile (blue circles and dash-dotted lines), and juvenilized (light blue squares and dashed lines) leaves of *P. tremula x alba* (A, D, G), *A. thaliana* (B, E, H), and *Z. mays* (C, F, I). Payback time and ROI are modeled using photosynthetic light response parameters and 12-hour light periods with constant PAR levels between 10 and 940 µmol m^2 s^1 and are plotted against the resulting daily integrated photosynthetic photon flux density (PPFD). Leaf lifespan data presented as means ± s.e.m. by solid symbols and individual replicates by transparent symbols. *P*-values determined by *ANCOVA* (A-C, G-I) or Student's *T* (D-F).

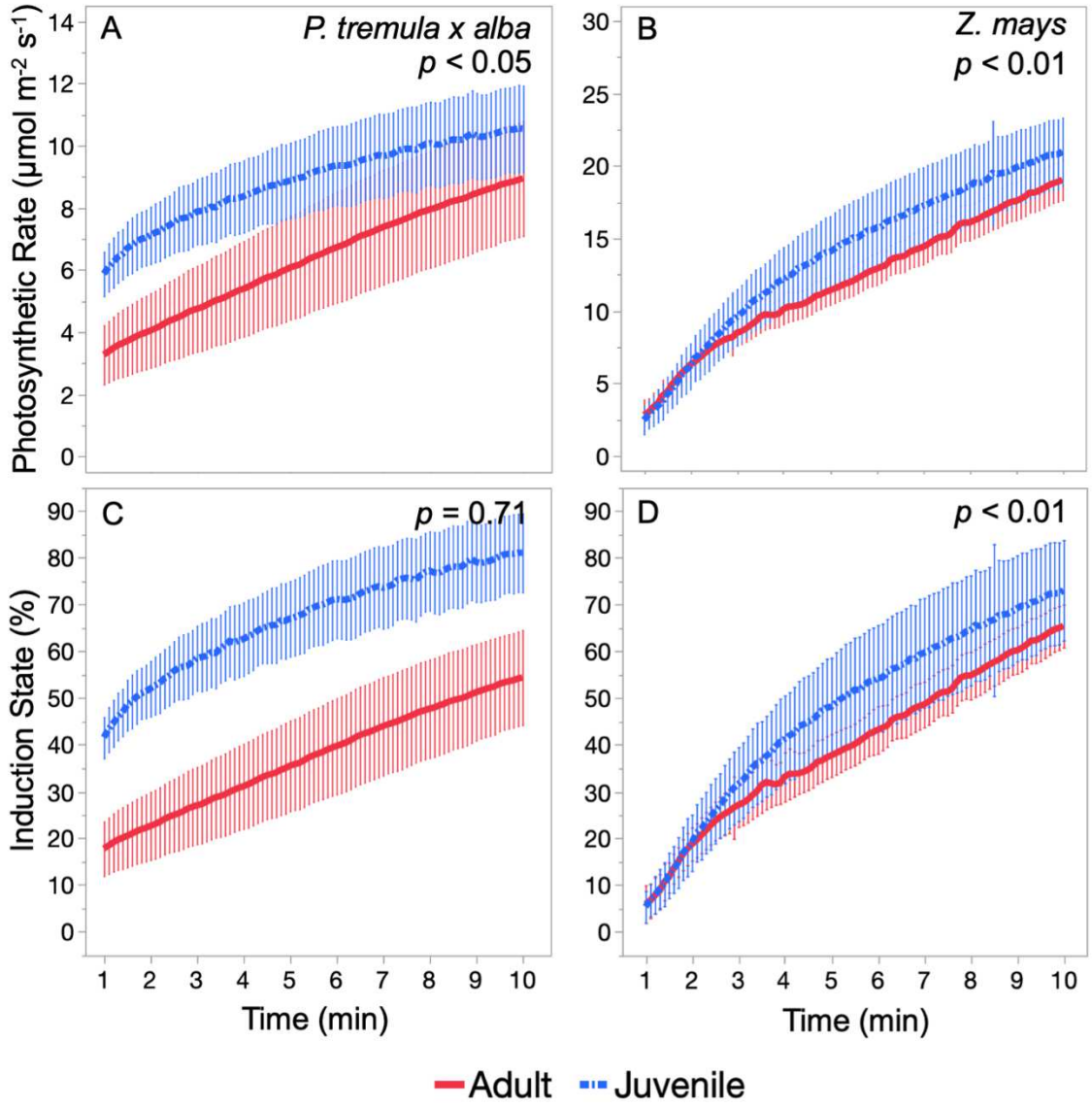

Figure 3. Photosynthetic rate and photosynthetic induction state during minutes 1-10 of exposure to saturating light for adult (solid, red) and juvenile (dash-dotted, blue) leaves of *P. tremula x alba* (A, C) and *Z. mays* (B, D). Data presented as the mean ± s.e.m. *P*-values determined by *ANCOVA.*

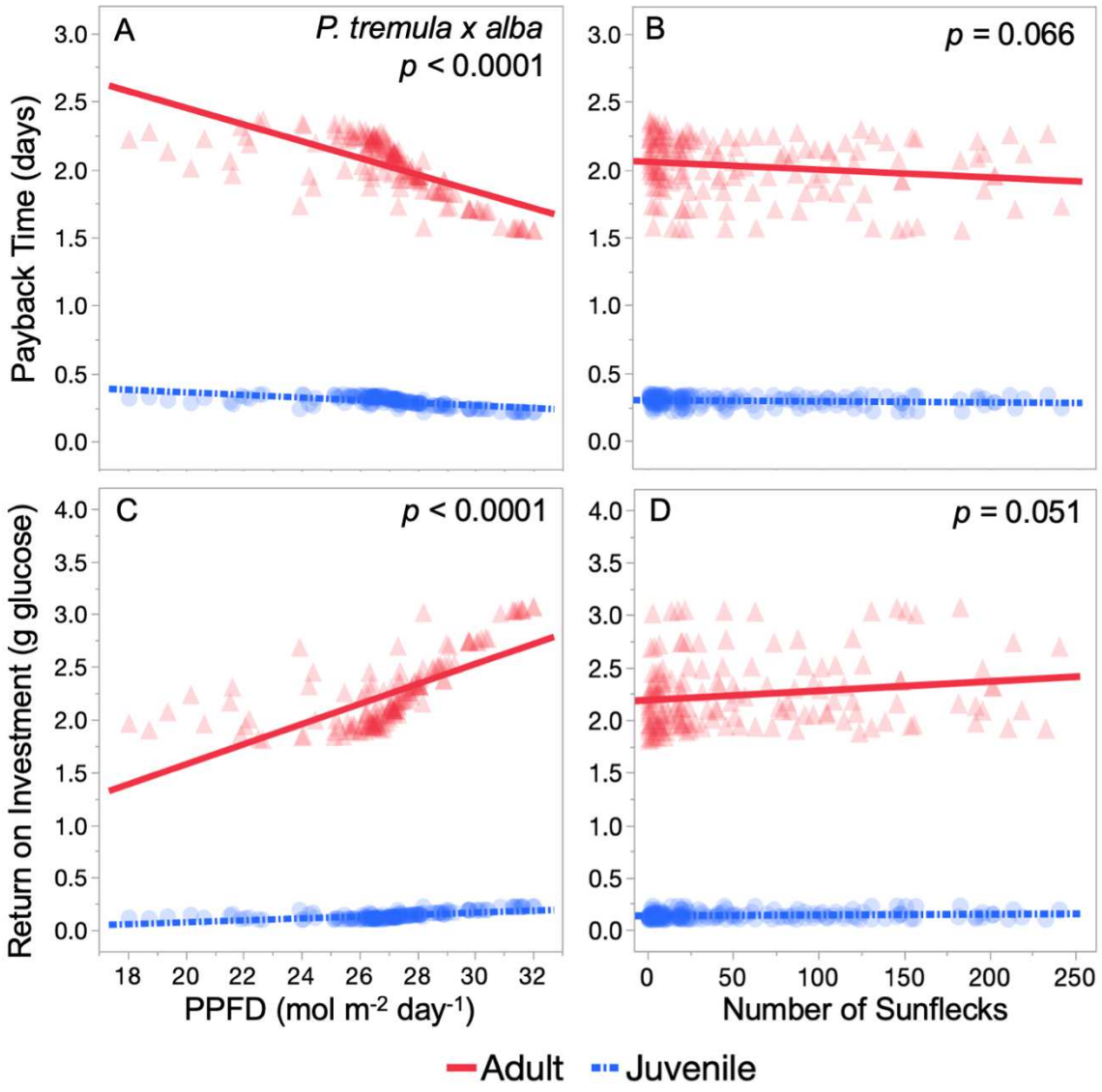

Figure 4. Leaf payback time (A-B) and return on investment (C-D) for adult (red triangles and solid lines) and juvenile (blue circles and dash-dotted lines) leaves from simulated dynamic light environments in *P. tremula x alba* plotted against daily integrated PPFD (A, C) and number of sunflecks across the day (B, D). Data presented as individual replicates by transparent symbols and linear line of best-fit. *P*-values determined by *ANCOVA*.

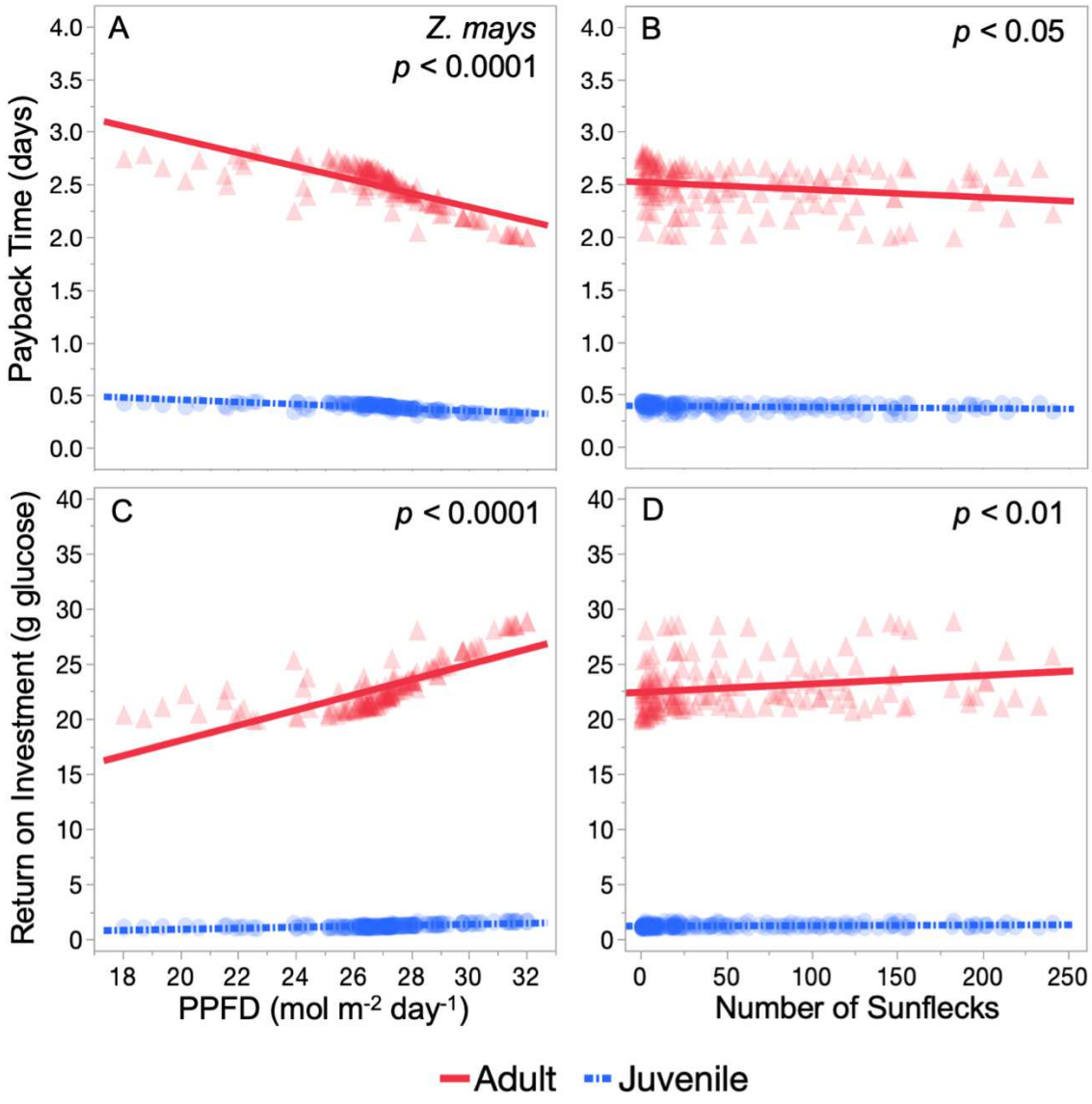

Figure 5. Leaf payback time (A-B) and return on investment (C-D) for adult (red triangles and solid lines) and juvenile (blue circles and dash-dotted lines) leaves from simulated dynamic light environments in *Z. mays* plotted against daily integrated PPFD (A, C) and number of sunflecks across the day (B, D). Data presented as individual replicates by transparent symbols and linear line of best-fit. *P*-values determined by *ANCOVA*.

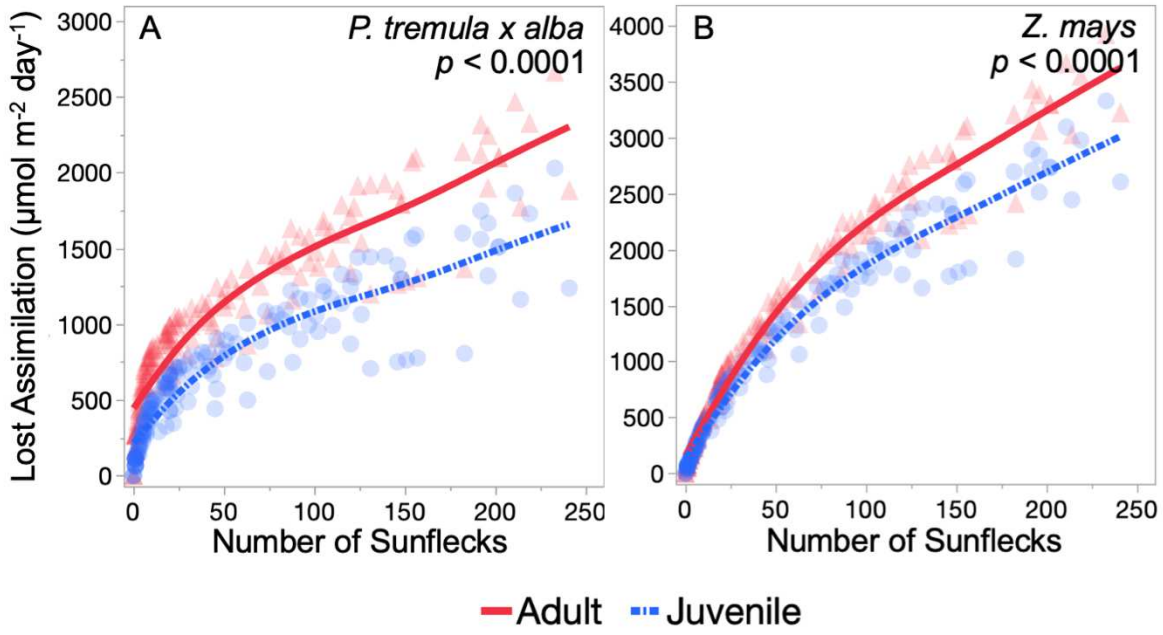

Figure 6. Lost assimilation due to slow photosynthetic induction in simulated dynamic light environments for adult (red triangles and solid line) and juvenile (blue circles and dash-dotted line) in *P. tremula x alba* (A) or *Z. mays* (B) plotted against number of sunflecks across the day. Data presented as individual replicates by transparent symbols and smoothed mean line. *P*-values determined by *ANCOVA*.

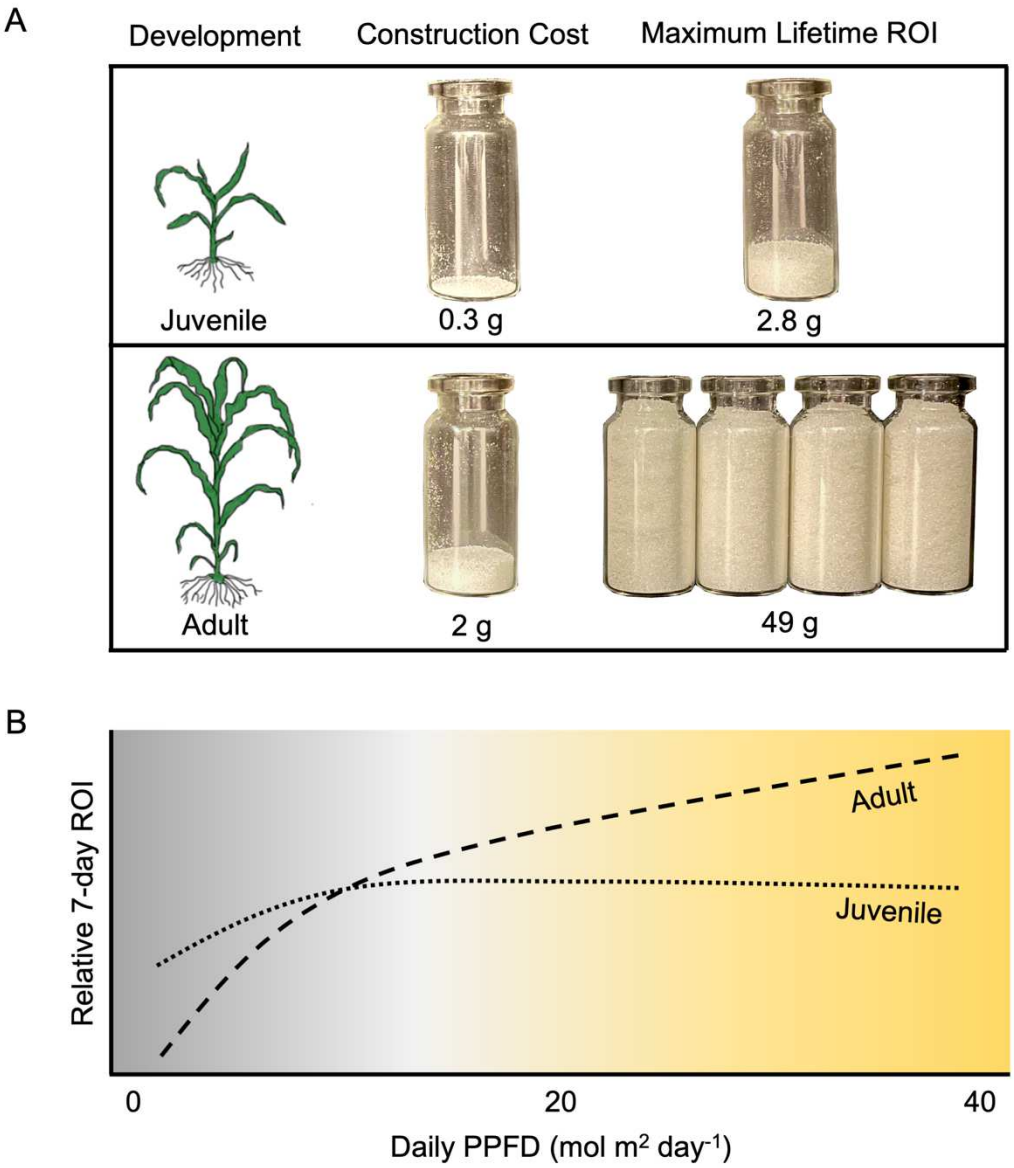

Figure 7. Juvenile leaves have a low-cost, low-return carbon economic strategy best suited for low-light environments while adult leaves have a high-cost, high-return strategy better suited for high light environments. Visual representations of the differences in construction cost and maximum lifetime return on investment (ROI), in grams of sugar, between juvenile and adult leaves of *Z. mays* (A). Maximum lifetime ROI was calculated using leaves photosynthesizing at light saturated photosynthetic rates for 12 hours a day during their full lifespan. Panel B shows the relative 7-day ROI for juvenile and adult leaves of *Z. mays* across light environments, depicting the advantage for the juvenile strategy in low-light (<10 mol m^2 day^{-1}) and adult leaves in high-light environments.

642

643

644 **Supplemental Tables**

645

646 **Table S1**. Leaf morphological traits

647 **Table S2.** Light response curve parameters

648 **Table S3.** Light induction parameters

649 **Table S4.** Linear relationships for carbon economic traits in simulated dynamic light

650 environments

651 **Table S5.** Inputs for each dynamic light simulation

652

653 **Supplemental Figures**

654

655 **Figure S1.** Per-gram leaf tissue payback time and return on investment relationships with daily

656 light

657 **Figure S2.** Dynamic light environment simulations

658 **Figure S3.** Per-gram leaf tissue payback time and return on investment for *P. tremula x alba*

659 from simulated dynamic light environments

660 **Figure S4.** Per-gram leaf tissue payback time and return on investment for *Z. mays* from

661 simulated dynamic light environments

Figures

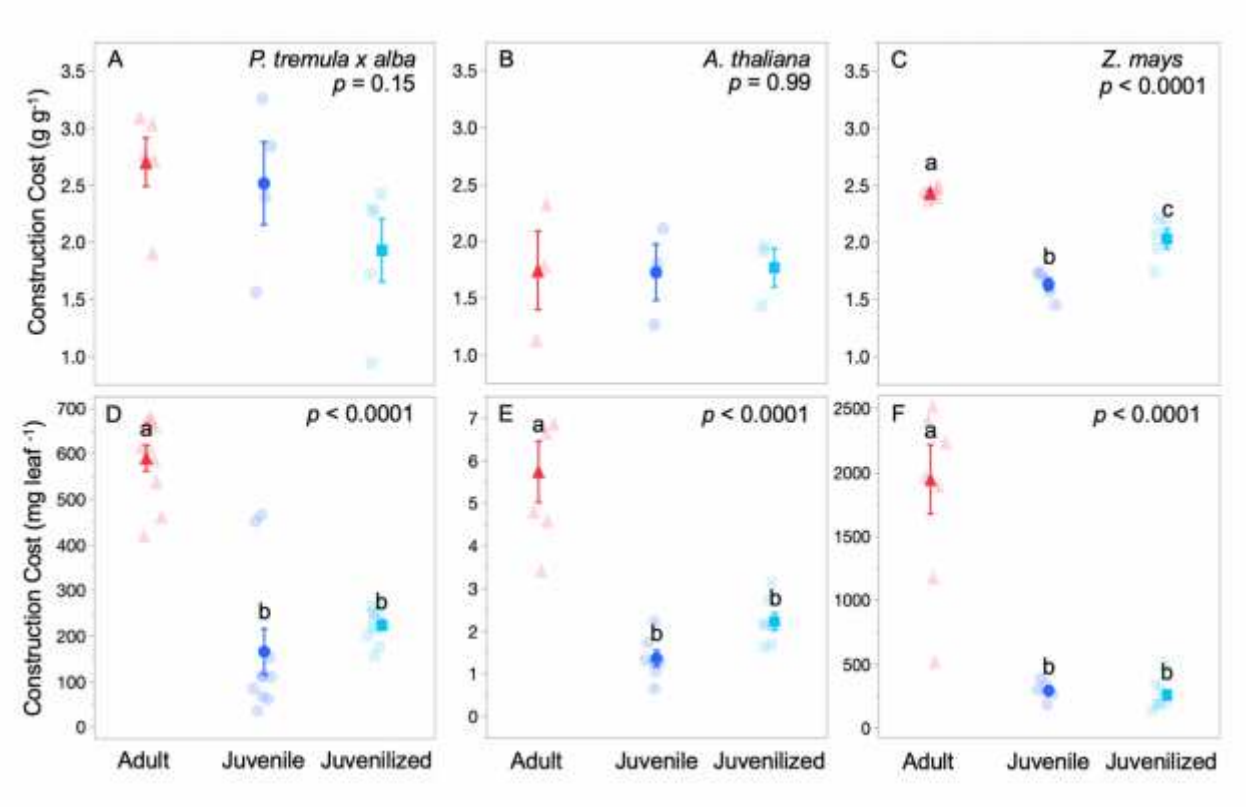

Figure 1

Please see the manuscript file to view the figure caption.

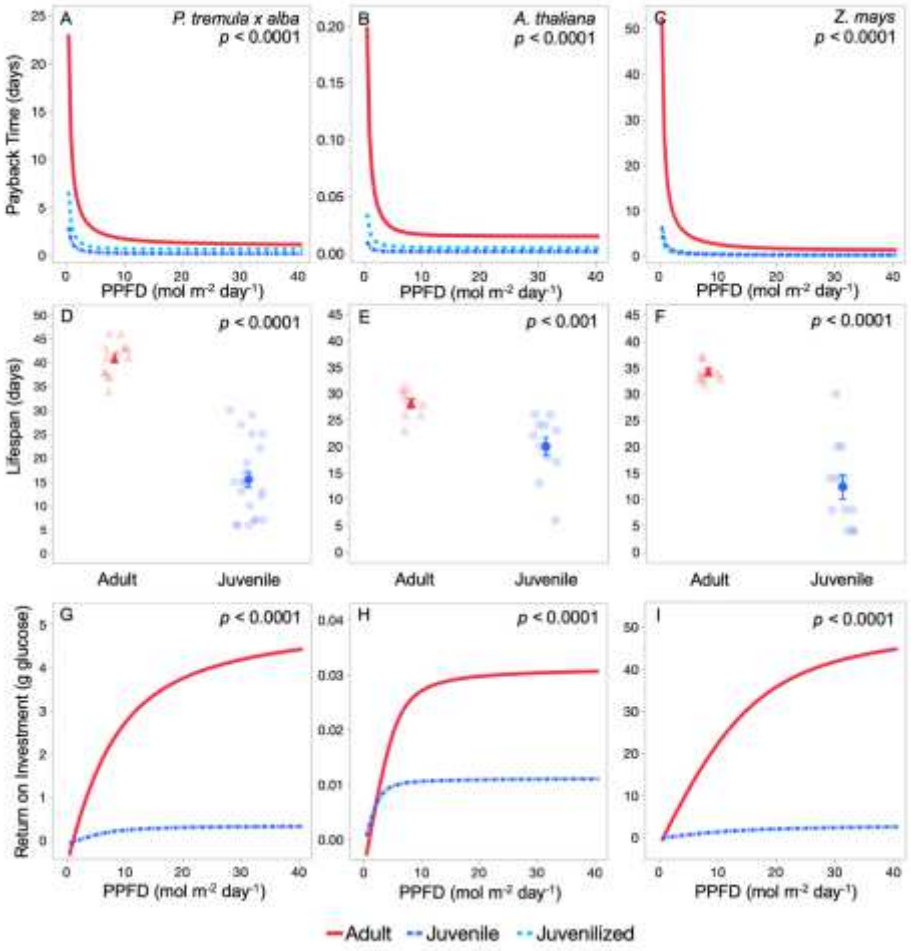

Figure 2

Please see the manuscript file to view the figure caption.

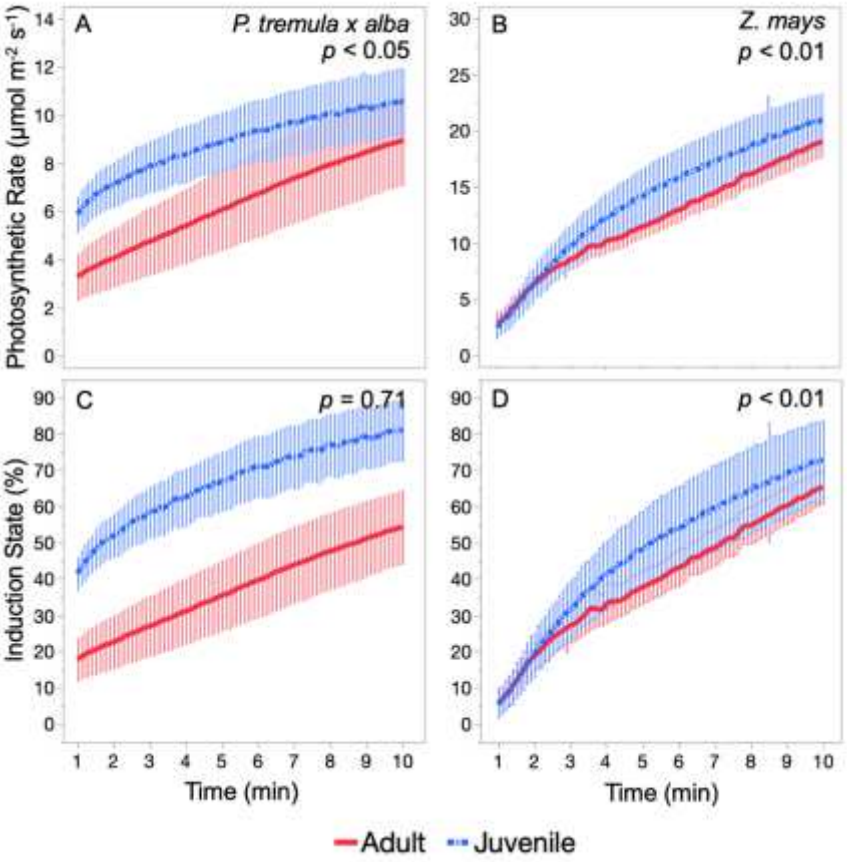

Figure 3

Please see the manuscript file to view the figure caption.

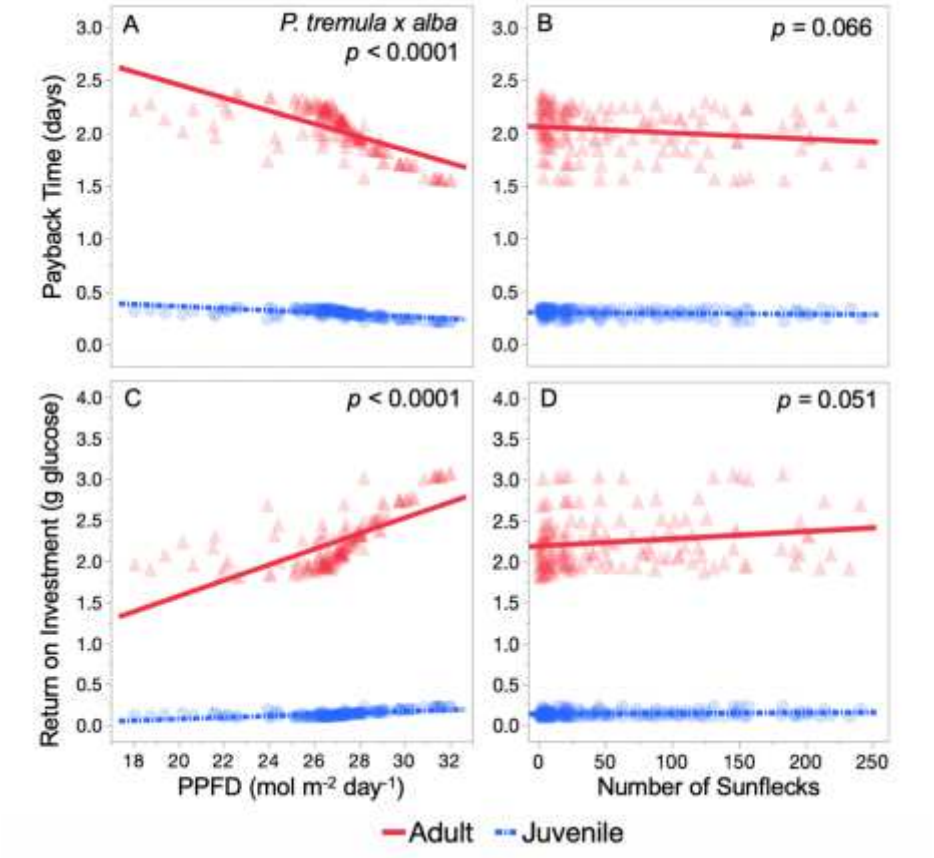

Figure 4

Please see the manuscript file to view the figure caption.

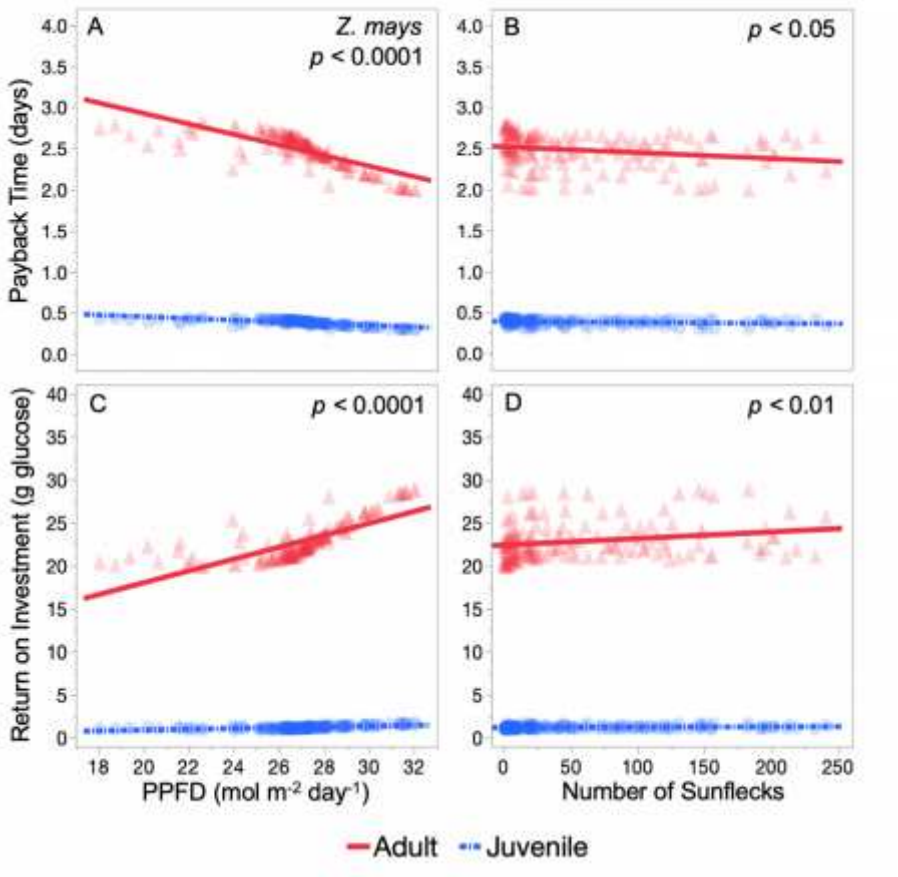

Figure 5

Please see the manuscript file to view the figure caption.

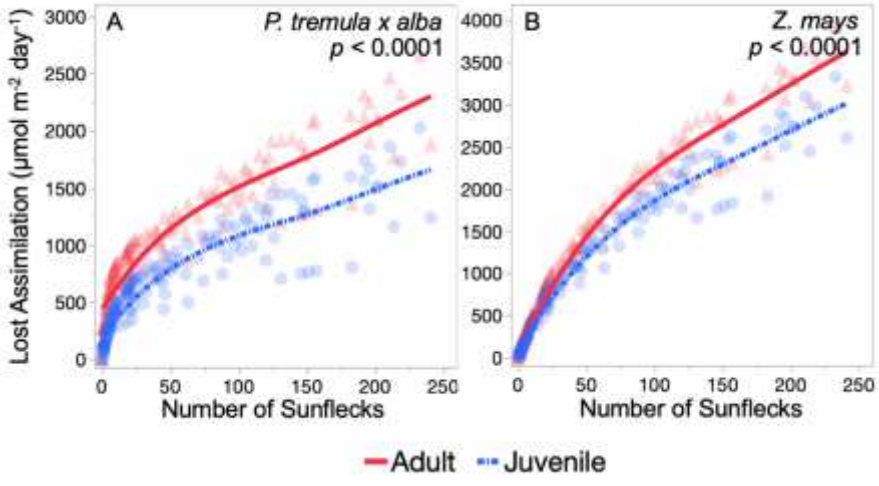

Figure 6

Please see the manuscript file to view the figure caption.

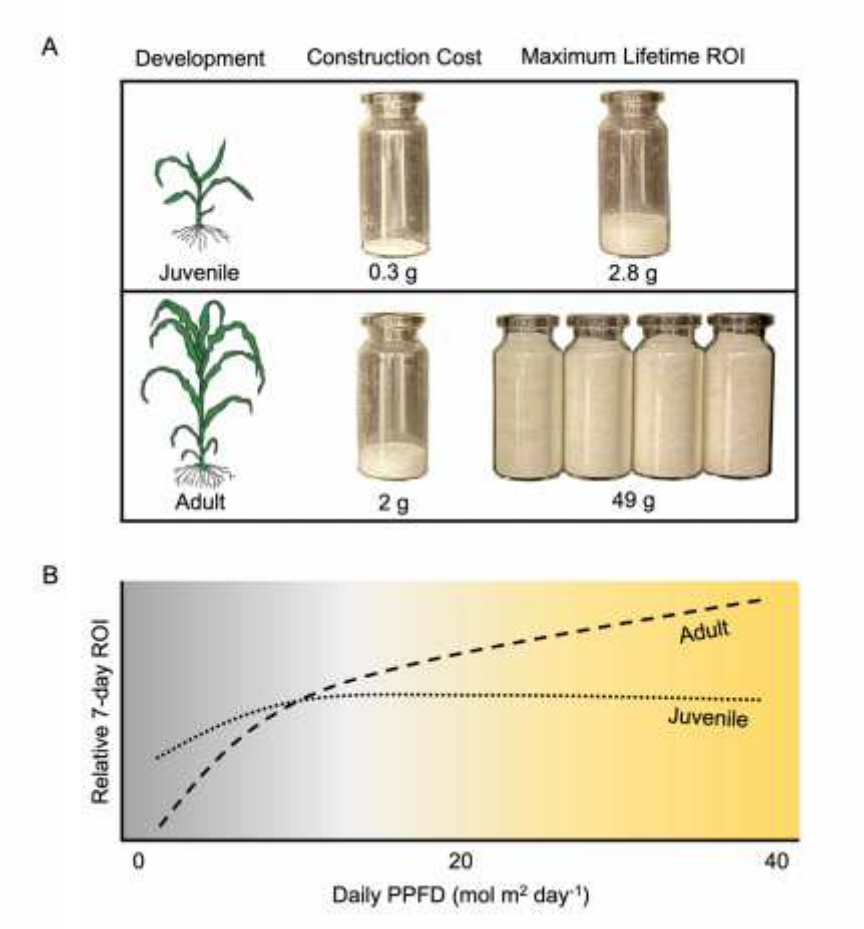

Figure 7

Please see the manuscript file to view the figure caption.

Supplementary Files

This is a list of supplementary files associated with this preprint. Click to download.

- Appendixequations.pdf
- Supplement.pdf